Luminescence behaviour of Eu^{3+} in hot-compressed silicate glasses

Cherbib, Mohamed Atef; Kapoor, Saurabh; Bockowski, Michal; Smedskjær, Morten Mattrup; Wondraczek, Lothar

Published in:
Journal of Non-Crystalline Solids: X

DOI (link to publication from Publisher):
10.1016/j.nocx.2019.100041

Publication date:
2019

Document Version
Publisher's PDF, also known as Version of record

Journal of Non-Crystalline Solids: X 4 (2019) 100041

Contents lists available at ScienceDirect

Journal of Non-Crystalline Solids: X

journal homepage: www.journals.elsevier.com/journal-of-non-crystalline-solids-x

Letter to the editor

Luminescence behaviour of Eu^{3+} in hot-compressed silicate glasses

Mohamed Atef Cherbib[a], Saurabh Kapoor[b], Michal Bockowski[c], Morten M. Smedskjaer[b], Lothar Wondraczek[a,*]

[a] Otto Schott Institute of Materials Research, University of Jena, Fraunhoferstrasse 6, 07743 Jena, Germany
[b] Department of Chemistry and Bioscience, Aalborg University, 9220 Aalborg, Denmark
[c] Institute of High-Pressure Physics, Polish Academy of Sciences, 01-142 Warsaw, Poland

ARTICLE INFO

Keywords:
Silicate glasses
Hot-compressed glasses
Trivalent europium
Luminescence

ABSTRACT

This paper aims to explore density-driven effects on the luminescence of Eu^{3+} doped silicate glasses. For this, mildly densified samples were fabricated by quasi-isostatic hot compression at up to 2 GPa from melt-quenched precursor materials. As a result of compression, both density and glass transition temperature of the blank (Eu free) and doped compositions increase. Raman spectroscopy indicates a slight increase in the intensity of vibrational modes assigned to small silicate rings and Si-O-Si bridges. Photoluminescence experiments reveal the creation of new paths of de-excitation, reducing the relative intensity of the transitions in the excitation spectra and the lifetime of the $^5D_0 \rightarrow {}^7F_2$ emission line. Meanwhile, the luminescence intensity remains unchanged due to enhanced oscillator strength and refractive index at uniform electron-phonon coupling strength. Luminescence spectra also show a slight expansion of some of the energy levels of Eu^{3+}, together with an increase of the bandwidth of the $^5D_0 \rightarrow {}^7F_2$ emission line due to the crystal-field influence and growing electron population of the lower Stark sub-levels. Finally, increasing symmetry of Eu^{3+} sites was detected with increasing degree of compaction, resulting in a reduction of the intensity of the forced electric dipole transition of $^5D_0 \rightarrow {}^7F_2$ relative to the magnetic dipole transition of $^5D_0 \rightarrow {}^7F_1$.

1. Introduction

Pressure-induced modifications present an additional degree of freedom to tailor the physical properties of amorphous materials [1]. Depending on the applied temperature during a compression experiment, significant amounts of network compaction and pressure-induced property variations can be obtained by mild treatment, i.e., in the pressure range below 1–2 GPa [2,3]. For oxide glasses, these modifications can be detected on the basis of structural analyses, for example, by monitoring changes in the speciation of the network-forming cations (e.g., Si^{4+}, B^{3+} or Al^{3+}), modifications of network topology, changes in the proportion of non-bridging oxygens, or variability in the occurrence of superstructural units [1,4–10]. In turn, these structural effects affect the macroscopic properties, e.g., Young's modulus, indentation hardness, and chemical durability [1,5,7,11–15].

High-pressure experiments on glasses are typically done at room temperature, enabling densification (to some extent reversible upon decompression) at very high pressure, often in the range of 10–100 GPa. Hot-compression, on the other hand, enables permanent densification (glasses remain in their densified state unless they are reheated to around the glass transition temperature, T_g) already at moderate pressure (~100–1000 MPa) when the glass is simultaneously heated in the vicinity of T_g [1]. Of particular interest, this latter approach enables the preparation of larger, homogeneously compacted specimens, so that pressure-induced variations of macroscopic properties as well as spectroscopic analyses are more readily accessible [1].

Besides mechanical and chemical properties, densification also impacts the radiative and non-radiative properties of luminescent ions and the phonon energy of their corresponding host lattice [16,17]. This includes a decrease in the distance between active ions and their ligands, or between activator and sensitizer species, thus affecting the statistics of activator clustering and associated quenching effects [18]. Through affecting ligand bond length and geometrical arrangement, pressurization may directly act on the magnitude of the local crystal field surrounding the luminescent centers, and, thus, affect the position of the energy levels, the splitting of the Stark sublevels, or the activation of otherwise forbidden intra-configurational electric dipole transitions by the Laporte selection rule. Indeed, the nephelauxetic effect induced by network compaction may increase the oscillator strength of these transitions, what can be an interesting route to boost the intensity

* Corresponding author.
E-mail address: lothar.wondraczek@uni-jena.de (L. Wondraczek).

https://doi.org/10.1016/j.nocx.2019.100041
Received 23 May 2019; Received in revised form 19 August 2019; Accepted 26 August 2019
Available online 15 November 2019

of the absorption lines of rare earth ions [16,19].

Due to these different aspects of sensitivity, the luminescence behaviour of active ions has received much attention for probing pressure-induced structural variations. Such experiments have been performed on various crystalline and amorphous hosts doped with rare earth or transition metal ions, as reviewed in Refs. [16, 17] and references therein. However, studies on the effect of hot-compression on the luminescence behaviour of glasses are scarce. For example, even though Eu^{3+} is one of the most-studied luminophores at ambient pressure or when embedded in cold-compressed matrices [20–26], there are no reports on its fluorescence or absorption line variations as a result of hot-compression treatment. Indeed, trivalent europium is often used as an active ion in optical thermometry or photonic devices; its non-degenerate ground state $^7F_0$ and excited state $^5D_0$ give easily interpreted luminescence and absorption spectra [27,28]. In addition, the characteristic occurrence of the hypersensitive forced electric dipole transition of $^5D_0 \rightarrow {}^7F_2$ ($\sim$ 612 nm) has made the Eu^{3+} ion a well-studied probe for examining variations on local ligand symmetry in disordered materials [29,30].

Considering all the attributes of Eu^{3+} as a probe and active ion, we now investigate hot compression-induced effects on the luminescence behaviour of a Eu^{3+}-doped silicate glass. Starting from the pressure-driven changes in density, glass transition temperature and structure (using Raman spectroscopy) of doped and blank samples, we explore the radiative and non-radiative properties of trivalent europium ions using steady state luminescence, time-resolved luminescence, and phonon sideband spectroscopy techniques. This is done in order to obtain insight into the local structure of the dopant and on the electron-phonon coupling strength of the host matrix.

2. Materials and methods

2.1. Glass preparation

Silicon dioxide, magnesium oxide, calcium carbonate, sodium carbonate, potassium carbonate, and europium oxide with high purity (*p.a.*) were selected as starting materials for glass preparation. The undoped matrix glass had the composition of (wt%) 71.94 SiO_2•5.64 MgO•9.23 CaO•13.17 Na_2O•0.02 K_2O, while the two doped glasses contained an additional 700 and 2000 ppm of Eu_2O_3, respectively. In the following, the samples are denoted SG*x*, whereby *x* indicates the dopant concentration of Eu_2O_3 in wt.-ppm. The specific matrix glass was chosen as representative for the most common types of alkali-alkaline earth silicate glasses. The relatively low europium concentrations were selected to avoid undesirable clustering of Eu^{3+} ions and, thus, luminescence quenching phenomena upon densification [18]. The batch materials were ground in a porcelain mortar and transferred to a platinum crucible. The batch was then heated progressively up to 1500 °C, melted for 2 h, poured into a graphite mould and annealed at the glass transition temperature of the parent glass.

2.2. Hot-compression

Compression procedures have been detailed in previous reports [1,12,13]. Here, glass samples were quenched from high pressures at well-controlled cooling rates in order to be able to distinguish between thermal and pressure-induced effects. To access the onset of pressure-induced structural alterations of the system, experiments were carried-out in the intermediate pressure regime, which also enabled the use of relatively large samples. Compression experiments were performed at pressures of up to 2 GPa in a cold seal pressure vessel. The samples were loaded directly into the vessel, and nitrogen gas was employed as the compression medium. The samples were equilibrated at a temperature around the glass transition temperature of the parent glasses for 30 min so that the equilibration time in these concomitant high-pressure and high-temperature experiments was well above the relaxation time of the glass and/or liquid.

Two nitrogen gas pressure chambers were used: one vertically positioned with an internal diameter of 6 cm for compression at 1 GPa and the other horizontally positioned with an internal diameter of 3 cm for compression at 2 GPa. A multi-zone and a single-zone cylindrical graphite furnace were used for compression at 1 and 2 GPa, respectively. To monitor the temperature during the experiments, PtRh6%–PtRh30% thermocouples were used. They were arranged in the furnaces and coupled with the input power control systems. In both cases, the pressure was measured by manganin gauges. The pressures and temperatures were stabilized with an accuracy of 1 MPa and 0.1 °C, respectively. Glass samples were placed in an alumina crucible and then heated in the furnaces inside the high-pressure reactors with a constant heating rate of 600 °C/h to the ambient pressure T_g value. The systems were kept at these conditions under high nitrogen pressure (1 or 2 GPa) for 30 min. Afterwards, the furnace was cooled down to room temperature at a constant rate of 60 °C/h, followed by decompression at a rate of 30 MPa/min.

2.3. Characterization

The density of the investigated glasses was obtained by the Archimedes' method at room temperature. Measurements were carried out on bulk samples and using distilled water as the immersion liquid. The glass transition temperatures T_g were measured via differential scanning calorimetry (DSC) using a Netzsch STA 449 Jupiter calorimeter with a heating rate of 10 °C/min under N_2 atmosphere with an accuracy of ± 2 °C.

Raman spectra were recorded using a Renishaw InVia Raman microscope operating at the laser excitation wavelength of 514.5 nm. The spectra were recorded for wavenumbers ranging from 100 to 1450 cm^{-1} with a resolution of 2 cm^{-1}.

Luminescence spectra were recorded using a high-resolution spectrofluorometer (Fluorolog, Horiba Jobin-Yvon). Time-resolved luminescence measurements were performed on the same device using a 70 W Xe flash lamp as the excitation source and time-correlated single photon counting (TCSPC). For the luminescence decay analyses, the excitation and emission wavelengths were fixed at 392 and 611 nm, respectively, and the raw data were fitted using a double-exponential function to obtain the average lifetime.

3. Results

Starting densities and the degree of densification of the blank and doped compositions are presented in Table 1. The densities of the three glasses (i.e., 0, 700, and 2000 ppm Eu_2O_3) increase uniformly from

Table 1
Density, densification percentage and glass transition temperature of the blank and Eu^{3+} doped glasses.

	SG0			SG700			SG2000		
	Ambient	1GPa	2GPa	Ambient	1GPa	2GPa	Ambient	1GPa	2GPa
Density (g/cm^3) ± 0.002	2.563	2.630	2.683	2.562	2.629	2.681	2.568	2.635	2.684
% of densification	–	2.60	4.67	–	2.62	4.68	–	2.61	4.53
T_g (± 2 °C)	533	545	545	539	545	541	530	545	541

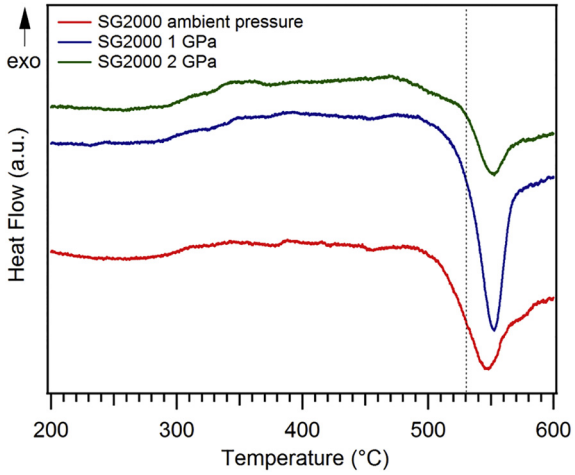

Fig. 1. DSC curves of as-prepared (ambient pressure) and hot-compressed SG2000 glasses.

2.56 g/cm^3 (ambient pressure) to 2.63 g/cm^3 (1 GPa) and then to 2.68 g/cm^3 (2 GPa). The degree of densification is around 2.6% and 4.6% at 1 GPa and 2 GPa, respectively, for both the blank and doped glass series.

The variation of T_g of the blank and doped samples is presented in Table 1. Corresponding DSC data are given in Fig. 1. For all samples, T_g increases by roughly 5–10°C as a result of compaction.

Raman spectra of the blank and doped compositions are presented in Fig. 2. The presented spectra were normalized to the area of the band at around 780 cm^{-1}. Considering first the low-frequency region between 400 and 700 cm^{-1}, we observe two bands at ~ 490 and 624 cm^{-1}, known as the defect lines D_1 and D_2, which can be related to the symmetric breathing vibration of the four- and three-membered silicate rings, respectively [31]. The band at about 546 cm^{-1} is assigned to the bending vibration of Si-O-Si bridges [31,32]. In the mid-frequency range between 700 and 900 cm^{-1}, the band at ~ 780 cm^{-1} corresponds to the symmetric stretching vibrations of Si-O-Si bridges [31,32]. In the high-frequency range between 900 and 1300 cm^{-1}, the bands at about 955 and 1090 cm^{-1} are related to the asymmetric stretching vibrations of Si—O bonds embedded in the metasilicate (Q^2) and disilicate (Q^3) species, respectively [31,32].

There are no notable shifts in the Raman band positions of the three base glasses upon densification. However, the bands´ relative intensities in the low- and high-frequency ranges are affected by the hot compression treatment. That is, the bands related to metasilicates and disilicates increase slightly with pressure. The same is seen even more pronouncedly for the low-frequency bands assigned to silicate rings and Si-O-Si bridges.

Normalized excitation spectra of the doped compositions (recorded using an emission wavelength of 611 nm) are provided in Fig. 3a-b. The spectra show the transitions of Eu^{3+} ions starting from the $^7F_0$ ground state toward the excited energy levels $^5G_4$,$^5D_4$,$^5G_2$, $^5L_6$,$^5D_3$,$^5D_2$,$^5D_1$ and $^5D_0$ at 362, 375, 380, 392, 413, 464, 525 and 578 nm, respectively. The spectra also display transitions starting from the thermally populated energy level $^7F_1$ toward $^5L_6$,$^5D_1$ and $^5D_0$ energy levels around 399, 532 and 586 nm [27].

Normalized luminescence spectra (recorded using an excitation wavelength of 392 nm) are also reported in Fig. 3c-d. They show the emission lines of Eu^{3+} ions starting from the $^5D_0$ excited level to the ^7F_j ground manifold, $^7F_0$, $^7F_1$, $^7F_2$, $^7F_3$ and $^7F_4$ energy levels at ~ 578, 591, 611, 653 and 703 nm, respectively [27].

Time-resolved luminescence data are presented in Fig. 3e-f; lifetimes of the $^5D_0 \rightarrow {}^7F_2$ transition are listed in Table 2. For the analyses, the excitation and emission wavelengths were fixed at 392 and 611 nm, respectively. For the SG700 glasses, the lifetime decreases from 2.55 ms

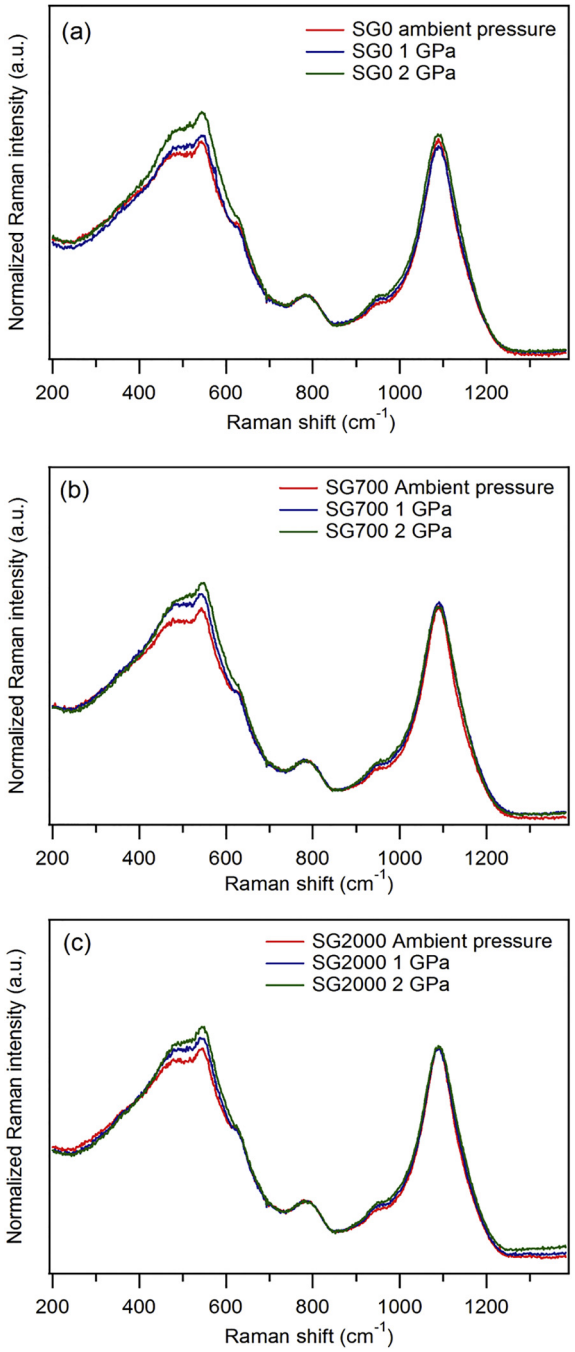

Fig. 2. Raman spectra of the blank and doped samples for both annealed and compressed glasses: (a) blank, (b) 700 ppm Eu_2O_3, and (c) 2000 ppm Eu_2O_3.

to 2.38 and 2.30 ms as a result of hot-compression at 1 GPa and 2 GPa, respectively. Likewise, for the SG2000 glass series, the lifetime is reduced from 2.63 ms in the pristine sample to 2.58 and 2.49 ms, respectively.

Table 2 further presents the bandwidth of the $^5D_0 \rightarrow {}^7F_2$ transition and the asymmetry ratio $R = I(^5D_0 \rightarrow {}^7F_2)/I(^5D_0 \rightarrow {}^7F_1)$ [28] (calculated using the intensity of the $^5D_0 \rightarrow {}^7F_2$ over that of the $^5D_0 \rightarrow {}^7F_1$ emission lines). The $^5D_0 \rightarrow {}^7F_2$ transition is an induced hypersensitive electric dipole transition, whose intensity is influenced by the local symmetry of Eu^{3+} cations. On the other hand, the $^5D_0 \rightarrow {}^7F_1$ transition is a magnetic dipole transition and its intensity is independent of the local environment of Eu^{3+}. The electron-phonon coupling strength g of the host matrix is also listed in Table 2. This latter value was calculated using the areas of the zero phonon line (which appears at 463 nm in the

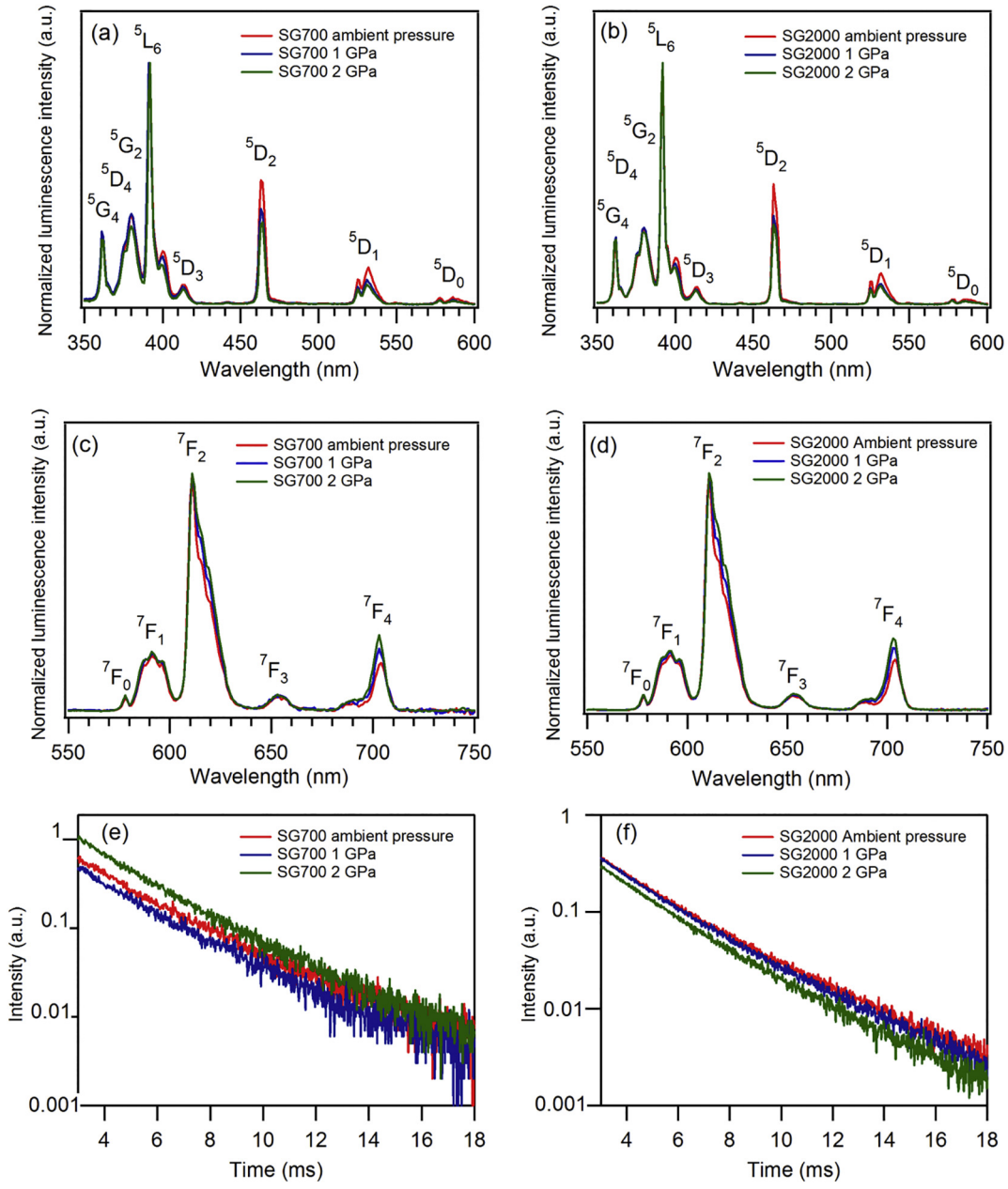

Fig. 3. Photoluminescence excitation spectra for λ_{em} = 611 nm (a,b), luminescence spectra for λ_{ex} = 392 nm (c,d) and luminescence decay (e,f) of the annealed and hot-compressed SG700 and SG2000 glasses.

Table 2
Bandwidth, asymmetry ratio (*R*), lifetime of the [5]$D_0 \rightarrow {}^7F_2$ transition and electron-phonon coupling (*g*) of the doped glass compositions.

	SG700			SG2000		
	Ambient	1GPa	2GPa	Ambient	1GPa	2GPa
FWHM of $^5D_0 \rightarrow {}^7F_2$ (nm)	9.21	11.46	12.24	9.33	11.58	12.32
Asymmetry ratio (*R*)	4.24	4.12	3.96	4.32	4.07	3.98
Lifetime (ms)	2.55	2.38	2.30	2.63	2.58	2.49
Electron-phonon coupling (*g*)	0.013	0.015	0.014	0.0126	0.013	0.012

excitation spectra) and of the phonon sideband associated with the almost pure electric dipole $^7F_0 \rightarrow {}^5D_2$ transition (which appears at about 440 nm [33,34]). Bandwidth, *R* and *g* parameters all change consistently when the glasses are hot-compressed: an increase occurs in the bandwidth of the $^5D_0 \rightarrow {}^7F_2$ emission line with pressure, as well as a decrease in the lifetime and in the asymmetry ratio. However, the electron-phonon coupling strength remains constant for both dopant concentrations.

4. Discussion

On a macroscopic scale, hot-compression increases the density and the glass transition temperature of the investigated glasses. This is in accordance with previous studies [3]. The overall degree of compaction which is achieved at 2 GPa corresponds to about one third of the maximum degree of compression of a typical soda lime silicate glass with similar former-to-modifier ratio.

On super-structural scale, compression reduces the distances between active ions and their ligands in the host matrix. This enhances the probability of interaction between ligands and 4f electrons by penetration of the ligand electron clouds into the ion configurations and/or

by covalent admixture of the 4f electrons with the ligand orbitals [16,17]. These interactions expand the oscillator strengths of the transitions, making them more allowed. In our study, even though the Raman spectra do not exhibit notable variations and the degree of densification is low, these interactions are already visible. This is probably due to the increasing crystal field strength and the nephelauxetic effect caused by compression. Together, these effects contribute to a slight increase in the intensity of the absorption lines of Eu^{3+}, reduce the lifetime of the $^5D_0 \rightarrow {}^7F_2$ transition as shown in Table 2, and influence the intensity of the emission lines.

In addition to oscillator strength, also the phonon energy of the host matrix plays a role in the lifetime variation. The evolution of the phonon energy can be observed by an uptick in the amplitude of Raman bands versus pressure, as shown in Fig. 2. Indeed, losses by non-radiative processes are expected to increase when the glasses are compressed due to the creation of new de-excitation paths, which alter the photoluminescence quantum yield and simultaneously the transitions´ lifetimes [16,17,28]. These new paths of de-excitation can also be detected when observing the declining intensity of the photoluminescence excitation lines for both doped glasses (Fig. 3, a and b).

Meanwhile, the regularity of emission lines for both doped samples versus pressure (Fig. 3c-d) is interesting, since room temperature densification (at high pressure) often reduces the luminescence intensity [16,17].

The fluorescence is also influenced by the expected increase in refractive index upon densification [1], and by the invariance of electron-phonon coupling (Table 2). The fact that the values of *g* do not change with pressure suggests that the vibration of the host glass perceived locally by the active ions is not strongly pressure-dependent. This corroborates earlier findings according to which hot-compression results in decoupled relaxation reactions on short and longer-range order [3]. Since the ion concentration in the studied glasses is low, the *g* factor can be considered as a reliable parameter [35]. While Raman spectroscopy probes the average phonon energy of the host, the local vibrational energy of the site in which Eu^{3+} ions are embedded can be better assessed using phonon sideband spectroscopy [35]. On the basis of the present observations, we suggest that all the above factors counterbalance the decrease in luminescence intensity (such as commonly observed in room temperature compression experiments) by compensating the losses through non-radiative processes.

Our results can also be used to understand in which sites the active ions are embedded and how hot-compression affects the splitting of the Eu^{3+} energy levels and Stark sublevels. Indeed, Fig. 3a-d show a slight blueshift of some of the transitions upon high-temperature densification of the samples. This indicates an expansion of Eu^{3+} energy levels, rarely observed during room temperature compression [16]. While such features are not easily understood in the absence of further data, we may discuss them from a simplistic viewpoint of glass structure [16]. Considering that the Eu^{3+} ions are smaller than the Ca^{2+} ions (1.21 vs. 1.26 Å for eightfold coordination [37]) and that trivalent europium species are embedded in the voids of the silicate network at ambient pressure, the availability of free volume may be larger in the vicinity of europium ions. Upon densification, this excess free volume is consumed without causing a notable change in the silicate backbone (denoted *congruent compaction* [36]); the glasses are compacted homogeneously as a function of applied pressure. In this case, one would expect increasing site symmetry, such as seen on the decrease in the asymmetry ratio with degree of compaction (Table 2). Finally, the increase in bandwidth of the $^5D_0 \rightarrow {}^7F_2$ emission line upon hot-compression can be explained by a growth in the electron population of the lower stark sublevels and, at the same time, increasing crystal field strength.

5. Conclusion

We investigated the effects of hot-compression at moderate pressure on the luminescence behaviour of Eu^{3+} ions embedded in a silicate glass matrix. Density and T_g measurements supported by vibrational spectroscopy confirmed densification of the silicate network without distinct structural variations. This densification influences the luminescence of Eu^{3+} in multiple ways: the oscillator strength increases, new paths of de-excitation are created, and variations occur in the forced hypersensitive electric dipole transitions. All three effects were observed on the lifetime of the $^5D_0 \rightarrow {}^7F_2$ emission line and on the intensities of the transitions as seen in the excitation spectra. However, the overall luminescence intensity of the $^5D_0 \rightarrow {}^7F_J$ emission lines was preserved, partly due to the expected increase in refractive index, and partly because of constant electron-phonon coupling strength. On a more general perspective, these findings suggest that the radiative and non-radiative properties of luminescent centers are not affected similarly by hot- versus cold-compression. Such understanding - if corroborated by further investigations using different matrices and different luminescent ions - can be used when applying Eu^{3+} and similar ions as structural probes, but also in the design of photonic devices with enhanced emission bandwidth and spectral coverage.

Declaration of Competing Interest

The authors declare that they have no known competing financial interests or personal relationships that could have appeared to influence the work reported in this paper.

Acknowledgment

The authors would like to thank the European Research Council (ERC) under the European Union's Horizon 2020 research and innovation program (ERC grant UTOPES, grant agreement no. 681652) for funding this work. M.M.S. acknowledges funding from the Independent Research Fund Denmark under Sapere Aude: DFF-Starting Grant (1335-00051A).

References

[1] S. Kapoor, L. Wondraczek, M.M. Smedskjaer, Pressure-induced densification of oxide glasses at the glass transition, Front. Mater. 4 (2017) 1–20, https://doi.org/10.3389/fmats.2017.00001.
[2] L. Wondraczek, H. Behrens, Y. Yue, J. Deubener, G.W. Scherer, Relaxation and glass transition in an isostatically compressed diopside glass, J. Am. Ceram. Soc. 90 (2007) 1556–1561, https://doi.org/10.1111/j.1551-2916.2007.01566.x.
[3] L. Wondraczek, H. Behrens, Molar volume, excess enthalpy, and Prigogine-Defay ratio of some silicate glasses with different (P,T) histories, J. Chem. Phys. 127 (2007) 154503, , https://doi.org/10.1063/1.2794745.
[4] M. Guerette, M.R. Ackerson, J. Thomas, F. Yuan, E.B. Watson, D. Walker, L. Huang, Structure and properties of silica glass densified in cold compression and hot compression, Sci. Rep. 5 (2015) 1–10, https://doi.org/10.1038/srep15343.
[5] T.K. Bechgaard, A. Goel, R.E. Youngman, J.C. Mauro, S.J. Rzoska, M. Bockowski, L.R. Jensen, M.M. Smedskjaer, Structure and mechanical properties of compressed sodium aluminosilicate glasses: role of non-bridging oxygens, J. Non-Cryst. Solids 441 (2016) 49–57, https://doi.org/10.1016/j.jnoncrysol.2016.03.011.
[6] M.B. Østergaard, R.E. Youngman, M.N. Svenson, S.J. Rzoska, M. Bockowski, L.R. Jensend, M.M. Smedskjaer, Temperature-dependent densification of sodium borosilicate glass, RSC Adv. 5 (2015) 78845–78851, https://doi.org/10.1039/c5ra16219j.
[7] K. Januchta, M. Bauchy, R.E. Youngman, S.J. Rzoska, M. Bockowski, M.M. Smedskjaer, Modifier field strength effects on densification behavior and mechanical properties of alkali aluminoborate glasses, Phys, Rev. Mater. 1 (2017) 1–12, https://doi.org/10.1103/PhysRevMaterials.1.063603.
[8] S. Kapoor, X. Guo, R.E. Youngman, C.L. Hogue, J.C. Mauro, S.J. Rzoska, M. Bockowski, L.R. Jensen, M.M. Smedskjaer, Network glasses under pressure: permanent densification in modifier-free Al_2O_3-B_2O_3-P_2O_5-SiO_2 systems, Phys. Rev. Appl. 7 (2017) 1–16, https://doi.org/10.1103/PhysRevApplied.7.054011.
[9] B. Mantisi, S. Adichtchev, S. Sirotkin, L. Rafaelly, L. Wondraczek, H. Behrens, C. Marcenat, N.V. Surovtsev, A. Pillonnet, E. Duval, B. Champagnon, A. Mermet, Non-Debye normalization of the glass vibrational density of states in mildly densified silicate glasses, J. Phys. Condens. Matter 22 (2010) 025402, , https://doi.org/10.1088/0953-8984/22/2/025402.
[10] S. Fuhrmann, T. Deschamps, B. Champagnon, L. Wondraczek, A reconstructive polyamorphous transition in borosilicate glass induced by irreversible compaction, J. Chem. Phys. 140 (2014) 054501, , https://doi.org/10.1063/1.4863348.
[11] S. Sawamura, R. Limbach, H. Behrens, L. Wondraczek, Lateral deformation and defect resistance of compacted silica glass: quantification of the scratching hardness of brittle glasses, J. Non-Cryst. Solids 481 (2018) 503–511, https://doi.org/10.

1016/j.jnoncrysol.2017.11.035.
[12] Y. Yue, L. Wondraczek, H. Behrens, J. Deubener, Glass transition in an isostatically compressed calcium metaphosphate glass, J. Chem. Phys. 126 (2007) 144902, , https://doi.org/10.1063/1.2719194.
[13] L. Wondraczek, S. Sen, H. Behrens, R.E. Youngman, Structure-energy map of alkali borosilicate glasses: effects of pressure and temperature, Phys. Rev. B 76 (2007) 014202, , https://doi.org/10.1103/PhysRevB.76.014202.
[14] B. Martin, L. Wondraczek, J. Deubener, Y. Yue, Mechanically induced excess enthalpy in inorganic glasses, Appl. Phys. Lett. 86 (2005) 121917, , https://doi.org/10.1063/1.1895483.
[15] L. Wondraczek, S. Krolikowski, H. Behrens, Relaxation and Prigogine-Defay ratio of compressed glasses with negative viscosity-pressure dependence, J. Chem. Phys. 130 (2009) 204506, , https://doi.org/10.1063/1.3141382.
[16] T. Tröster, Optical studies of non-metallic compounds under pressure, in: K.A. Gschneidner, Jr.J.-C.G. Bünzli, V.K. Pecharsky (Eds.), Handbook on the Physics and Chemistry of rare Earths, 33 Elsevier, 2003, pp. 515–589, , https://doi.org/10.1016/S0168-1273(02)33007-1.
[17] K.L. Bray, High pressure probes of electronic structure and luminescence properties of transition metal and lanthanide systems, in: H. Yersin (Ed.), Transition Metal and Rare Earth Compounds, Excited States Transition, Interaction I, 213 Springer, 2001, pp. 1–94, , https://doi.org/10.1007/3–540-44447-5_1.
[18] G. Gao, J. Wei, Y. Shen, M. Peng, L. Wondraczek, Heavily Eu_2O_3-doped yttria-aluminoborate glasses for red photoconversion with a high quantum yield: luminescence quenching and statistics of cluster formation, J. Mater. Chem. C 2 (2014) 8678–8682, https://doi.org/10.1039/c4tc01447b.
[19] R. Reisfeld, C.K. Jorgensen, Lasers and Excited States of Rare Earths, Springer, Berlin Heidelberg, 1977, https://doi.org/10.1007/978-3-642-66696-4.
[20] G. Chen, J. Hölsä, J.R. Peterson, A luminescence study of single-crystal $EuPO_4$ at high pressure, J. Phys. Chem. Solids 58 (1997) 2031–2037, https://doi.org/10.1016/S0022-3697(97)00133-9.
[21] G. Chen, R.G. Haire, J.R. Peterson, Effect of pressure on amorphous $Eu(OH)_3$: a luminescence study, J. Phys. Chem. Solids 56 (1995) 1095–1100, https://doi.org/10.1016/0022-3697(95)00017-8.
[22] M.J. Lochhead, K.L. Bray, High-pressure fluorescence line narrowing of Eu(III)-doped sodium disilicate glass, Phys. Rev. B 52 (1995) 763–775, https://doi.org/10.1103/PhysRevB.52.15763.
[23] A. Monteil, C. Bernard, S. Chaussedent, M. Ferrari, N. Balu, J. Obriot, Pressure effect on the structure and the luminescence of rare-earth ions doped glasses: an investigation by molecular dynamics simulation, J. Lumin. 87–89 (2002) 691–693, https://doi.org/10.1016/s0022-2313(99)00360-9.
[24] C.K. Jayasankar, K.R. Setty, P. Babu, T. Tröster, W.B. Holzapfel, High-pressure luminescence study of Eu^{3+} in lithium borate glass, Phys. Rev. B 69 (2004) 214108, , https://doi.org/10.1103/PhysRevB.69.214108.
[25] N. Soga, K. Hirao, M. Yoshimoto, H. Yamamoto, Effects of densification on fluorescence spectra and glass structure of Eu^{3+}-doped borate glasses, J. Appl. Phys. 63 (1988) 4451–4454, https://doi.org/10.1063/1.340165.
[26] A. Vlasic, D. Sevic, M.S. Rabasovic, J. Krizan, S. Savic-Sevic, M.D. Rabasovic, M. Mitric, B.P. Marinkovic, M.G. Nikolic, Effects of temperature and pressure on luminescent properties of Sr_2CeO_4:Eu^{3+} nanophosphor, J. Lumin. 199 (2018) 285–292, https://doi.org/10.1016/j.jlumin.2018.03.061.
[27] K. Binnemans, Interpretation of europium (III) spectra, Coord. Chem. Rev. 295 (2015) 1–45, https://doi.org/10.1016/j.ccr.2015.02.015.
[28] P.A. Tanner, Some misconceptions concerning the electronic spectra of tri-positive europium and cerium, Chem. Soc. Rev. 42 (2013) 5090–5101, https://doi.org/10.1039/c3cs60033e.
[29] L. Wondraczek, Z. Pan, T. Palenta, A. Erlebach, S.T. Misture, M. Sierka, M. Micoulaut, U. Hoppe, J. Deubener, G.N. Greaves, Kinetics of decelerated melting, Adv. Sci. 5 (2018), https://doi.org/10.1002/advs.201700850.
[30] G. Gao, L. Wondraczek, Spectral asymmetry and deep red photoluminescence in Eu^{3+}-activated $Na_3YSi_3O_9$ glass ceramics, Opt. Mater. Express 4 (2014) 476–485, https://doi.org/10.1364/OME.4.000476.
[31] A.K. Yadav, P. Singh, A review of the structures of oxide glasses by Raman spectroscopy, RSC Adv. 5 (2015) 67583–67609, https://doi.org/10.1039/C5RA13043C.
[32] P.F. McMillan, Structural studies of silicate glasses and melts-applications and limitations of Raman spectroscopy, Am. Mineral. 69 (1984) 622–644.
[33] S. Gopi, S.K. Jose, A. George, N.V. Unnikrishnan, C. Joseph, P.R. Biju, Luminescence and phonon sideband analysis of Eu^{3+} doped alkali fluoroborate glasses for red emission applications, J. Mater. Sci. Mater. Electron. 29 (2018) 674–682, https://doi.org/10.1007/s10854-017-7961-8.
[34] P. Suthanthirakumar, S. Arunkumar, K. Marimuthu, Investigations on the spectroscopic properties and local structure of Eu^{3+} ions in zinc telluro-fluoroborate glasses for red laser applications, J. Alloys Compd. 760 (2018) 42–53, https://doi.org/10.1016/j.jallcom.2018.05.153.
[35] M. Dejneka, E. Snitzer, R.E. Riman, Blue, green and red fluorescence and energy transfert of Eu^{3+} in fluoride glasses, J. Lumin. 65 (1995) 227–245, https://doi.org/10.1016/0022-2313(95)00073-9.
[36] B.P. Rodrigues, S. Sen, L. Wondraczek, Pressure-induced chemical reordering in supercooled polyionic sulfophosphate liquids, J. Non-Cryst. Solids 499 (2018) 95–100, https://doi.org/10.1016/j.jnoncrysol.2018.07.019.
[37] R.D. Shannon, Revised effective ionic radii and systematic study of inter atomic distance in halides and Chalgogenides, Acta Cryst. A 32 (1976) 751–767, https://doi.org/10.1107/s0567739476001551.